Chinese Journal of Chemical Engineering 81 (2025) 270–276

Contents lists available at ScienceDirect

Chinese Journal of Chemical Engineering

journal homepage: www.elsevier.com/locate/CJChE

Full Length Article

Effect of carbon modifications on the performance of hydrogenation catalysts

Zhenhui Lv [1, 2, #], Jianan Li [1, #], Tao Yang [2], Yibao Li [3], Chong Peng [1, *]

[1] State Key Laboratory of Fine Chemicals, School of Chemical Engineering, Dalian University of Technology, Dalian 116024, China
[2] Dalian Research Institute of Petroleum and Petrochemicals, SINOPEC, Dalian 116041, China
[3] Key Laboratory of Organo-Pharmaceutical Chemistry, Gannan Normal University, Ganzhou 341000, China

ARTICLE INFO

Article history:
Received 14 October 2024
Received in revised form
8 December 2024
Accepted 15 December 2024
Available online 19 March 2025

Keywords:
Hydrogenation
Catalyst
Reactivity
Petroleum
Fixed-bed

ABSTRACT

In the petroleum industry, the properties of catalysts play a crucial role in the performance of hydroprocessing reactions. Carbon modification can effectively regulate the physicochemical properties of catalysts, but further in-depth research is necessary. In this study, ethylene glycol was used as the carbon source to investigate the impact of varying carbon amounts on the performance of the Mo-Ni/Al_2O_3 hydrogenation catalyst. The results showed that both the pore structure and surface hydroxyl groups of catalysts can be adjusted after carbon modification. As the carbon content increased, the surface acidity of catalysts gradually decreased, and the interaction between carrier and active metal gradually weakened, leading to more octahedral coordination in form of polynuclear polymolybdic acid. The dispersion and sulfidation degree of Mo species improved, ultimately resulting in more hydrogenation active phases. Consequently, the catalyst exhibited enhanced hydrodesulfurization (HDS) and hydrodenitrification (HDN) activities.

1. Introduction

With the continuous tightening of environmental protection standards, the pace of clean diesel upgrading is accelerating, and restrictions on the content of polycyclic aromatic hydrocarbons (PAHs) are becoming increasingly stringent [1,2]. The latest *Worldwide Fuel Charter* recommends that, for markets with advanced emission control requirements (*e.g.*, the United States, China, and Europe), the mass fraction of PAHs in diesel fuel should not exceed the reference value of 2% [3]. Consequently, producing diesel with lower polycyclic aromatic hydrocarbon has become not only a trend towards cleaner oil products but also one of the significant challenges faced by modern oil refining industries.

The hydrorefining process can hydrogenate and saturate PAHs in diesel fuel into monocyclic aromatic hydrocarbons or naphthenes, thereby reducing PAHs content and improving diesel quality [4,5]. This process is a crucial and effective technology for producing clean diesel, with the catalyst playing a decisive role in the hydrogenation and saturation reaction activity, as well as in the distribution of the resulting products [6]. Hydrogenation catalysts typically consist of active metal components (*e.g.* Ni, Co, Mo) and carriers (*e.g.* Al_2O_3, CeO_2) [7,8]. Compared to metal oxidation carriers (such as alumina), carbon carriers supports interact more weakly with active metals, which facilitates the formation of highly active type-II Ni(Co)-Mo-S phase during the sulfurization process [9–11]. Additionally, carbon carriers exhibit significantly improved resistance to carbon deposition, which aids in the hydrocracking of carbon-containing compounds into lighter hydrocarbons [12]. However, carbon carriers also present challenges that limit their industrial application. For example, the high microporosity of activated carbon hinders the diffusion of larger molecular, and its weak mechanical strength make it unsuitable for the high-pressure conditions typically in fixed-bed reactors [13]. Moreover, the relatively high cost of carbon nanotubes and mesoporous carbon prevents them from competing with the inexpensive and widely available alumina [12]. As a consequence, metal oxide carriers remain the dominant catalyst carriers in industrial market [14].

Although alumina remains widely used as a classic carrier for active metal components, its properties can be modified to influence the interaction between metals and carriers, thereby altering

* Corresponding author.
E-mail address: pengchong@dlut.edu.cn (C. Peng).
# These authors contributed equally to this work.

https://doi.org/10.1016/j.cjche.2024.12.025

the structure and properties of active metal phases [15,16]. Recently, one type of carbon-modified Al_2O_3 materials (CCA), produced by introducing carbon species onto the Al_2O_3 surface, has garnered significant attention. This modification not only preserves the thermal and mechanical properties of Al_2O_3 but also imparts the surface characteristics of carbon materials [17]. However, there is still insufficient information regarding the structure-activity relationship between carbon modification and hydrogenation activity.

Herein, ethylene glycol was selected as the carbon source to modify the hydrogenation catalyst, allowing for a comprehensive characterization of the evolution of the active phase structure. The hydrogenation activity of the carbon-modified catalyst was evaluated using Iranian vacuum wax oil as the target sample. The effects of varying carbon content on the hydrogenation performance of the catalysts were also investigated. This work provides valuable insights for the future development of high-performance hydrogenation catalysts.

2. Experimental

2.1. Chemical and materials

The alumina carrier used in this study has a cylindrical morphology and is of industrial grade. Ethylene glycol was obtained from Tianjin Guangfu Technology Development Co., Ltd. Other reagents were purchased from Sinopharm Chemical Reagent Co., Ltd., China. All reagents were of analytical grade and used without further purification. Ultra-pure deionized (DI) water (>18 $M\Omega \cdot cm^{-1}$) was generated by a Milli-Q system and used to prepare the various solutions in this work.

2.2. Preparation of catalysts

The blank reference catalysts were initially prepared by impregnating the industrial alumina carrier in the molybdenum-nickel-phosphorus solution using an equal-volume impregnation approach [18]. The impregnated carriers were then dried and calcined at 500 °C under a nitrogen atmosphere to obtain the Mo-Ni/Al_2O_3 catalyst, with a carbon content of 0% (designated as Cat-CB).

Subsequently, Mo-Ni/Al_2O_3 catalysts with varying levels of carbon modification were prepared using a similar method. Specifically, the molybdenum nickel phosphorus solution was mixed with different amounts of ethylene glycol to form a homogeneous impregnation solution. The industrial alumina carriers were impregnated in this molybdenum-nickel-phosphorus ethylene glycol solution, then dried and calcined at 500 °C under nitrogen to produce the carbon modified hydrogenation catalysts. Based on the measured carbon content of the resulting Mo-Ni/Al_2O_3 catalysts, the hydrogenation catalysts were labeled as follows: Cat-A (0.56%(mass)), Cat-B (0.98%(mass)), Cat-C (1.61%(mass)), and Cat-D (2.47%(mass)).

2.3. Characterizations

Temperature-programmed reduction (TPR) of catalysts were carried out on an AUTOCHEM II 2920 (Micromeritics, US). X-ray diffraction (XRD) characterizations were conducted on a D/Max-2400 (Rigaku Corporation, Japan) with Cu K_α radiation ($\lambda = 0.15418$ nm) at a scan rate of 1 (°) $\cdot min^{-1}$. *In situ* Raman spectra were collected on a DXR3 Raman Microscope (Thermo Fisher Scientific, US) by using the laser of 532 nm. X-ray photoelectron spectroscopy (XPS) of catalysts was conducted on a MULTILAB 2000 spectrometer (Thermo Fisher Scientific, US) with an Al K_α -ray source to characterize the surface chemical status of catalyst samples. The obtained results were calibrated with reference to the C 1s binding energy at 284.6 eV. The quantitative analysis on the sulfidation degree of the molybdenum species (denoted as Mo^{4+}, Mo^{5+}, and Mo^{6+}) and nickel species (denoted as Ni-Mo-S, NiO_x, NiS_x, and Ni shake up) could be obtained through the corresponding deconvoluted results for the Ni_{2p} and Mo_{3d} XPS spectra. The sulfidation degrees of molybdenum (S_{Mo}) for these catalysts are determined with $Mo^{4+}/(Mo^{4+}+Mo^{5+}+Mo^{6+})$, while the sulfidation degrees of nickel (S_{Ni}) are determined by the proportion of Ni sulfided species to the total Ni species [19,20]. High-resolution transmission electron microscopy (HR-TEM) were made using a JEM-2100 plus transmission electron microscope (JEOL Ltd., Japan). The infrared spectroscopy of CO adsorption was recorded on a Chemisorption-300 AUTOSORB-I-C chemisorption measurement (Quantachrome Instruments, US). The pore information of catalyst samples was analyzed on the ASAP 2405 physical adsorption analyzer (Micromeritics Inc. USA).

The sulfur content in the raw oil and products was determined by an ultraviolet fluorescence method (ANTEK-9000 Sulfur/Nitrogen Analyzer, Petroleum Analyzer Company L.P., USA), according to the recommended method of Petrochemical Industry Standard (SH/T 0689-2000, China). The operating conditions were presented as followed: the injector injection speed of 1 $\mu l \cdot s^{-1}$, the cracking furnace temperature of 1100 °C, the cracking oxygen flow rate of 500 $ml \cdot min^{-1}$, the inlet oxygen flow rate of 30 $ml \cdot min^{-1}$, and the carrier gas argon flow rate of 130 $ml \cdot min^{-1}$. The nitrogen content was analyzed by the method of oxidation combustion and chemiluminescence (ZDN-2000 Chemiluminescence Nitrogen Analyzer, Jiangsu New High-Tech Analytical Instrument Co., Ltd., China), according to the recommended method of Petrochemical Industry Standard (SH/T 0657—2007). The operating conditions were set as followed: the syringe injection amount of 20 μl, the cracking furnace temperature of 1050 °C, the cracking oxygen flow rate of 480 $ml \cdot min^{-1}$, the inlet oxygen flow rate of 60 $ml \cdot min^{-1}$, the ozone flow rate of 150 $ml \cdot min^{-1}$, and the carrier gas argon flow rate of 100 $ml \cdot min^{-1}$. Other property indicators of the raw oil and hydrogenated oil are measured according to the technical requirements and test methods specified in the adopted method of National Standard (GB 19147l—2016, CN).

2.4. Catalysis activity evaluation

To better simulate the real activity, the catalysts were presulfurized prior to catalysis evaluation using a home-made fixed-bed microreactor [21]. Aviation kerosene dissolved with CS_2 was used as the sulfurizing agent. The sulfurization process consisted of a three-stage temperature program: 230 °C for 4 h, 270 °C for 4 h and 340 °C for 3 h. The reaction pressure was maintained at 8.0 MPa with a hydrogen-to-oil feed volume ratio of 500:1.

Furthermore, the catalyst activity evaluation was conducted on a fixed-bed device. The carbon-modified catalysts (0.234—1.00 mm) were placed in the central section of the reactor, occupying a volume of 80 ml. Aviation kerosene dissolved with CS_2 was employed as the sulfurizing agent, and the vulcanization process followed a three-stage temperature program: 230 °C for 8 h, 270 °C for 8 h, and 340 °C for 8 h. Iranian vacuum wax oil was then used for evaluation, with its properties shown in Table S1. It was pumped into the reactor loaded with the catalyst for hydrogenation reaction. Then, the obtained products after hydronation catalysis entered into the stripping tower for stripping, after which they were collected in the product tank. The activity evaluation of the catalyst was performed at a hydrogen partial pressure of 8.0 MPa, a hydrogen-to-oil volume ratio of 500:1, a reaction temperature of 370 °C, and a volume space velocity of 1.0 h^{-1}.

In the petrochemical field, the reaction activity of hydrogenation catalyst is usually evaluated by the rate index of hydrodesulfurization rate (HDS, %) and hydrodenitrogenation (HDN, %). Their calculation method is shown as below:

$$\mathrm{HDS} = \frac{w_{S0} - w_{S1}}{w_{S0}} \times 100\%$$

$$\mathrm{HDN} = \frac{w_{N0} - w_{N1}}{w_{N0}} \times 100\%$$

where w_{S0} and w_{S1} represent the mass fractions ($\mu g \cdot g^{-1}$) of sulfur in the raw material and product, and w_{N0} and w_{N1} represent the mass fractions ($\mu g \cdot g^{-1}$) of nitrogen in the raw material and product, respectively.

3. Results and Discussion

To investigate the effect of carbon content, the pore structure of the catalysts with varying levels of carbon modification was comparatively analyzed (Tables S2–S3). As the carbon content increased, the specific surface area of the catalysts exhibited an increasing trend, while both the pore volume and pore size decreased (Table S2). According to the pore size distribution (Table S3), the percentage of pores with a diameter less than 6 nm gradually increased with higher carbon modification, while the proportion of pores with a diameter greater than 10 nm decreased. This suggests that carbon modification primarily blocks the micropores in the catalysts, with some carbon also filling the macropores. These findings indicate that the carbon modification shifts the pore size distribution of catalysts towards smaller pores.

The effects of carbon modification on the interaction between active metals and supports were further carried out by a H_2-TPR characterization of carbon-modified oxidation state catalysts (Fig. 1(a)). The prominent H_2 reduction peak was attributed to polynuclear polymolybdic acid, which features an octahedral coordination structure of molybdenum oxide in the catalyst and serves as a precursor to form the highly active Mo-Ni-S phase [22]. The main reduction peak position (~370 °C) of catalysts only slightly shifts towards high temperature after carbon modification. This phenomenon could be ascribed to the formation of Mo_2C species, which require a higher reduction temperature to reduction into Mo^{4+}. In addition, the introduction of carbon content might cause pore blockage in molybdenum and nickel species, resulting in a bit higher temperatures necessary to penetrate and enter the interior to reduce them. In particular, the area of main reduction peak (~370 °C) displays an increase tendency with the carbon content, indicating more abundant active metal sulfide phase induced after carbon modification. Referred from previous literature, the introduction of carbon modification could weaken the interaction force between alumina carrier and active metals, improving the dispersion and sulfidation of metal sites [23]. This results in the abundance of active metal phase

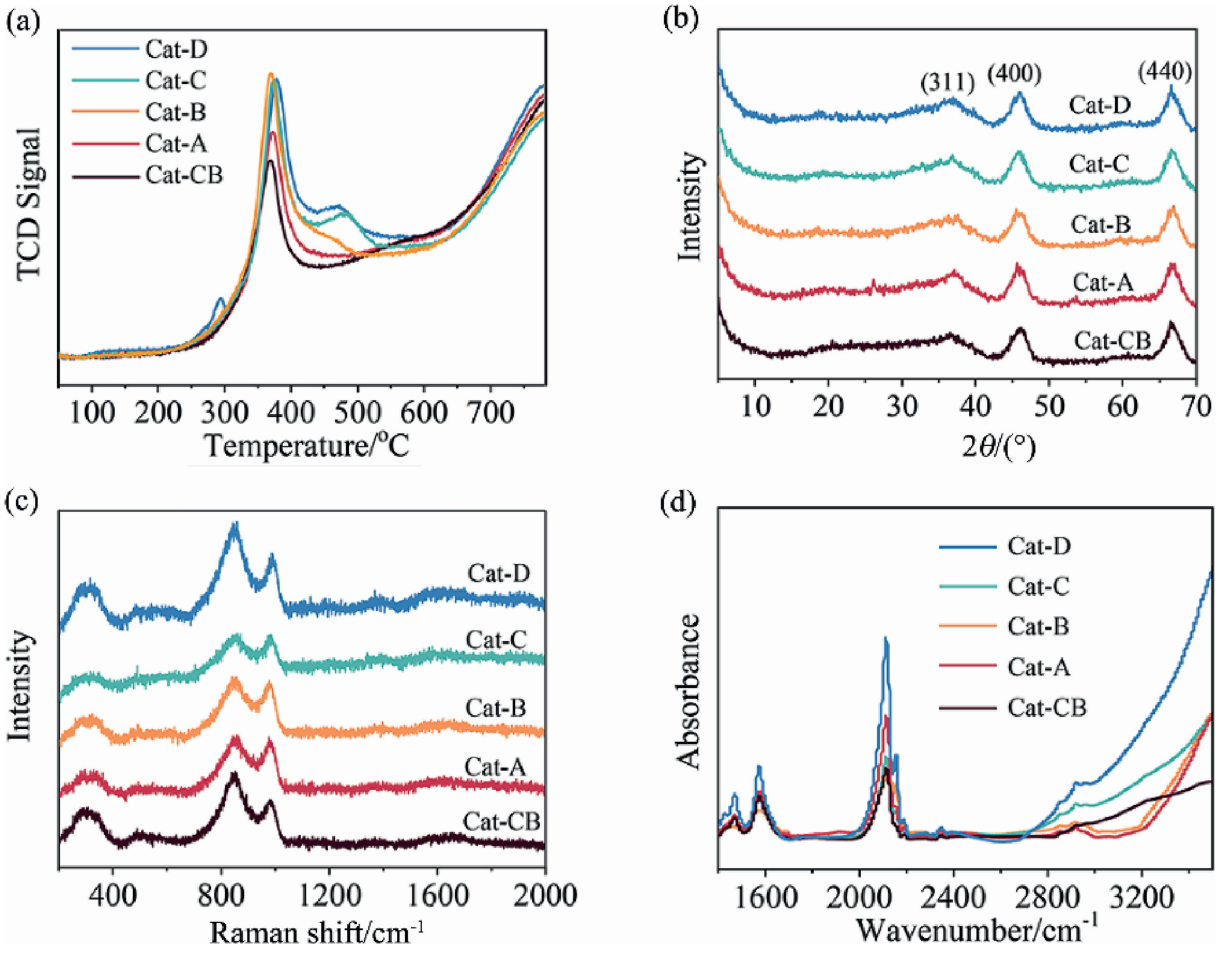

Fig. 1. (a) TPR curves, (b) XRD patterns, (c) Raman spectra, and (d) CO-IR patterns of catalysts modified with varyingcarbon content.

exposes on the catalyst, also proved by the increased H_2 reduction peak area after carbon modification. Once carbon modification reaches a certain level, another small reduction peak emerges surrounding 475–500 °C, indicating that the carbon-modified catalyst displayed more octahedral coordination polynuclear polymolybdic acid MoO_3. It reveals that the catalysts can form more highly active Mo-Ni-S phases after carbon introduction. Additionally, the XRD patterns (Fig. 1(b)) show characteristic peaks at 37.6°, 45.9° and 67.0° in the carbon-modified catalysts, which correspond to the (3 1 1), (4 0 0), and (4 4 0) diffraction planes of γ-Al_2O_3 (JCPDS No. 10-0425), respectively. No diffraction peaks of molybdenum oxide, nickel oxide or their composite oxides were observed in the XRD results. This suggests that all catalysts modified with varying carbon contents exhibited only γ-Al_2O_3 crystallinity, with the active metals present in a highly dispersed form or as small crystallites [24].

It has been previously reported that both the hydrogenation activity and anti-coking performance of catalyst are closely related to their surface acidity [25–27]. The characterization of the obtained catalysts (Table S4) revealed significant changes in the surface acidity of carbon-modified catalysts. As the carbon modification increased, the acid content on the catalyst surface decreased at 150–250 °C but increased at 400–500 °C. However, the total acid content on the catalyst surface gradually decreased. At lower temperatures, carbon-containing organic matter was not completely decomposed but rather carbonized, resulting in increased alkalinity and decreased acidity and hydrophilicity. This also facilitated the loading of active metals. At higher temperatures (400–500 °C), the complete decomposition of carbon-containing organic matter resulted in an increase in acid content, as most acidic hydroxyl groups on the alumina surface and hydroxyl groups of organic matter were exposed.

Raman spectra of different catalysts were also collected to investigate the changes of surface species. For the molybdenum oxide species, the content of MoO_4^{2-}, $Mo_7O_{24}^{6-}$ and $Mo_8O_{26}^{4-}$ species in the carbon modified catalysts displayed significant variations (Fig. 1(c)). The symmetric and asymmetric vibration bands of the terminal Mo=O double bond appeared in the ranges of 900–1000 cm^{-1} and 830–970 cm^{-1}, respectively. Additionally, the bending vibration of the terminal Mo=O double bond was observed in the range of 310–370 cm^{-1}. Two types of molybdenum oxide species were present in all five catalysts. The Raman scattering peaks corresponding to the symmetrical octahedral molybdenum oxide clusters $Mo_7O_{24}^{6-}$ were located at 330 and 850 cm^{-1}, while those assigned to the symmetrical octahedral molybdenum species $Mo_8O_{26}^{4-}$ appeared at 525 and 975 cm^{-1} [28]. The intensity of Raman signals reflects the abundance of corresponding species in the catalysts. As the carbon modification increased, the peak intensity of both $Mo_7O_{24}^{6-}$ and $Mo_8O_{26}^{4-}$ species increased, suggesting that carbon modification significantly weakens the interaction between the active metal and the support. Consequently, more symmetrical octahedral molybdenum oxides form on the catalyst surface. However, the tetrahedral molybdenum oxide MoO_4^{2-}, observed at 180 cm^{-1} in the catalysts, is likely attributed to the composite compound $Al_2(MoO_4)_3$, formed by the strong chemical interaction between molybdenum oxide and alumina, or the composite compound $NiMoO_4$ resulting from the strong chemical interaction between molybdenum oxide and nickel oxide. This is likely due to the high treatment temperature during the carbonization process, which facilitates the formation of the spinel phase [29].

To further characterize the surface states, CO adsorption infrared spectroscopy (CO-IR) was performed on the catalysts (Fig. 1(d)). According to previous literature, the characteristic peak of CO adsorption on Al^{3+} coordinatively unsaturated sites (CUS) appears at 2195 cm^{-1}, while the interaction with the acidic OH group of alumina results in a characteristic peak at 2150 cm^{-1}. Additionally, the characteristic peak of CO adsorption on the unpromoted Mo sites is observed at 2120 cm^{-1}, whereas the peaks on the promoted Ni sites are found at 2080 and 2050 cm^{-1}, corresponding to the mutual adsorption of CO on Ni and Mo sites in the active Ni-Mo-S phase [21]. All the catalysts exhibited a strong peak in the range of 2000–2200 cm^{-1}, with the peak intensity significantly increasing as the levels of carbon modification rose. This suggests that carbon introduction can effectively reduce the interaction between the support and active metal, greatly promoting the formation of more active Ni-Mo-S phases and enhancing the hydrogenation activity of catalysts.

Through the XPS characterization analysis, the chemical states of the active Mo and Ni species of carbon modified catalysts were investigated (Fig. 2(a) and (b)) and the sulfidation degrees of Mo and Ni in the catalyst were estimated (Table S5). The high resolution Mo_{3d} spectrum showed a multi-peak coupling superposition state, allowing for the identification of different species (Mo^{4+}, Mo^{5+} and Mo^{6+} species) after deconvolution. Specifically, the characteristic peaks of sulfurized Mo^{4+} species appeared as twin bands at 225.0 and 233.4 eV, while those of Mo^{6+} species presented twin bands at 232.4 and 237.8 eV. Additionally, the characteristic peaks assigned to Mo^{5+} species of O-Mo-S were located at 228.8 and 235.7 eV [30,31] Moreover, the characteristic peaks of Ni species could be deconvoluted in Ni $2p_{3/2}$ spectrum, in which Ni_xS_y (852.8 eV), Ni in the Ni-Mo-S phase (853.7 eV), and Ni in the oxygen surrounding (856.5 eV) could be identified [32]. According to the XPS data obtained from the spectra (Table S5), the relative amounts of the Ni speceis components in all investigated samples are compared. It shows that the peak area of Mo-Ni-S in the carbon-modified catalyst gradually increased with higher carbon content. This results indicates that the carbon-modified hydrogenation catalyst contained more active sulfided phases (*e.g.* Mo-Ni-S and MoS_2).

The sulfidation degrees of MoO_3 and NiO in the catalyst without carbon modification were estimated at 75.1% and 85.2%, respectively. However, with carbon modification, the sulfidation degrees increased as the carbon content rose. Specifically, the sulfidation degrees of MoO_3 were 77.6%, 78.6%, 81.2%, and 85.4%, while those of NiO were 87.3%, 87.5%, 88.9%, and 90.2% for Cat-A to Cat-D, respectively. The surface atomic ratio of metal determines the dispersion state of the active metals. The atomic ratio of Mo/Al on the catalyst surface without carbon modification was approximately 0.065, while that of Ni/Al was estimated to be 0.021. After carbon modification, both Mo/Al and Ni/Al atomic ratios improved (Table S6), indicating that Mo and Ni species exhibited better dispersion on the catalyst surface, which favors the formation of Ni-Mo-S phases. This enhanced dispersion can be attributed to the redistribution of oxidized hydroxyl groups in the carbon-modified hydrogenation catalyst, which weakens the interaction between the support and active metals, enhancing the dispersion and sulfidation of Mo and Ni species [28]. More notably, the presence of carbon delays the sulfidation of Ni species, significantly promoting the formation of MoS_2 and Mo-Ni-S active phases.

Moreover, after the sulfidation treatment, the catalyst surface exhibited a typical layered lamellar structure of MoS_2 and NiS. To observe these micro-level changes, HRTEM was used to characterize the catalyst surface (Fig. 3). The length and number of stacked layers of MoS_2 lamellae were analyzed and quantified for each catalyst (Table S7). The average slab length (L) and average stacking layer number (N) of MoS_2 were estimated using the following Eqs. (1) and (2):

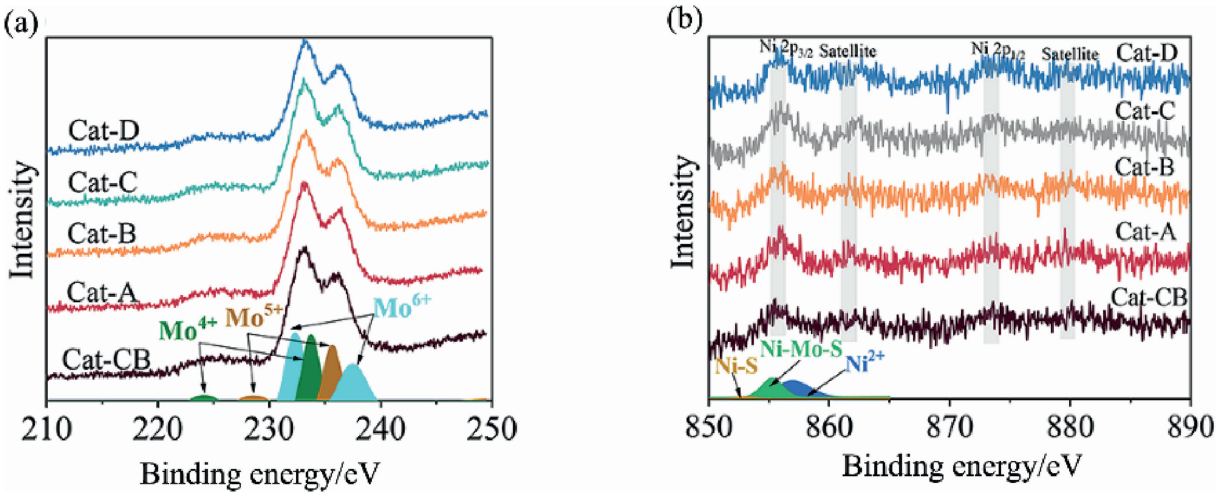

Fig. 2. XPS results of different carbon modified catalysts (a) Mo 3d, and (b) Ni 2p orbits.

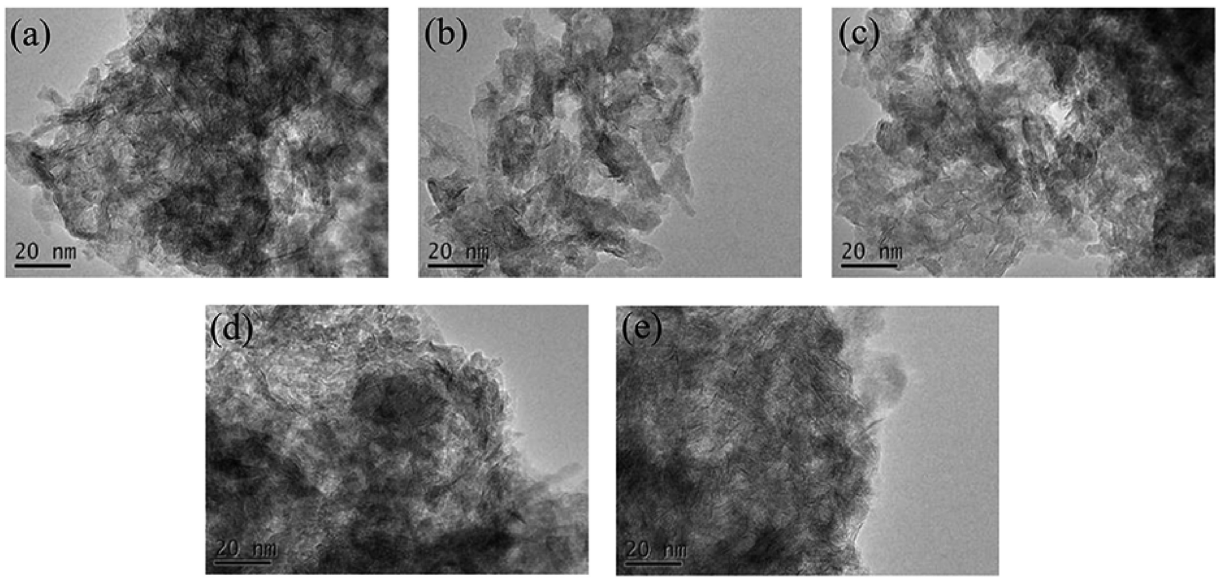

Fig. 3. TEM images of different carbon content modified catalysts: (a) Cat-CB, (b) Cat-A, (c) Cat-B, (d) Cat-C, and (e) Cat-D.

$$L = \frac{\sum_{i-1}^{n} S_i L_i}{\sum_{i-1}^{n} S_i} \quad (1)$$

$$N = \frac{\sum_{i-1}^{n} S_i N_i}{\sum_{i-1}^{n} S_i} \quad (2)$$

where L_i represents the sheet length of a MoS_2, N_i represents the stacking layer number of a MoS_2 unit, and S_i is the number of slabs or stacks in a determined range of length or stacking layer number.

From the results in Fig. 3 and Table S7, it is clear that the average length of MoS_2 lamellae in the blank reference catalyst was approximately 3.58 nm, with an average stacking layer number of 2.6. After carbon modification, the average length of MoS_2 lamellae in the sulfide catalyst increased significantly, along with a higher average stacking layer number. These trends became more pronounced as the amount of modified carbon content increased. This can be attributed to the ethylene glycol used as the carbon source, which forms a strong chelate with the active metal in the catalysts. Upon carbonization, the carbon wraps around the molybdate ions, creating an isolation effect on the active metal Mo species, which significantly improves their dispersion. Additionally, carbon modification enhances the distribution of hydroxyl groups on the catalyst surface, weakens the interaction between the carrier and active phases, prevents the aggregation of the active phase, and reduces the accumulation layer number of Mo species on the catalyst surface.

Finally, the hydrogenation activity of the carbon-modified catalyst was evaluated using a small fixed-bed test device. The middle section of the reactor was filled with the carbon-modified catalyst (0.71–1.00 mm, 80 ml). Jet fuel dissolved with CS_2 was used as the vulcanized oil. The sulfurization process followed a three-stage temperature program: 230 °C for 8 h, 270 °C for 8 h, and 340 °C for 8 h. Subsequently, Iranian vacuum wax oil was used to

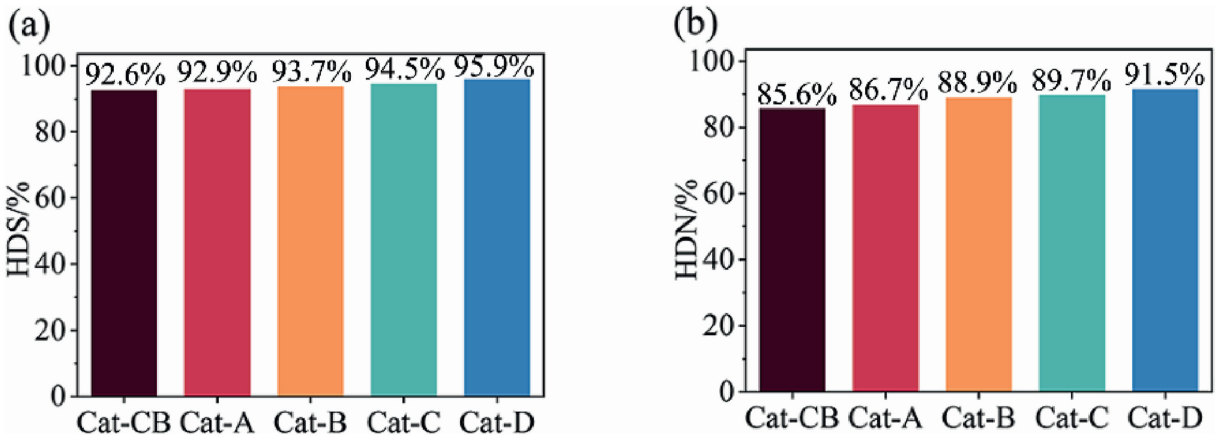

Fig. 4. Activities of different carbon content modified catalysts in (a) hydridesulfurization (HDS) and (b) hydridenitrogenation (HDN).

evaluate the hydrogenation performance whose properties are shown in Table S8. The activity of the catalyst was assessed under the following conditions: hydrogen partial pressure of 8.0 MPa, hydrogen-to-oil volume ratio of 500:1, reaction temperature of 370 °C, and volume space velocity of 1.0 h^{-1}. The HDS and HDN activities of catalysts modified with different amounts of carbon were evaluated under the same process conditions. As shown in Fig. 4, under identical conditions, the HDS and HDN activities of the carbon-modified catalysts were higher than those of the unmodified catalyst. Specifically, the activities improved with increasing carbon content, in which the hydrodesulfurization activities of Cat-CB, Cat-A, Cat-B, Cat-C, and Cat-D were 92.6%, 92.9%, 93.7%, 94.5%, and 95.9%, respectively. Additionally, the HDN activities of these catalysts followed a similar trend, increaing with greater carbon modification.

4. Conclusions

Overall, this work employed a carbon-modification strategy to enhance the properties and activity of hydrogenation catalysts. The carbon-modified hydrogenation catalyst promoted the formation of more octahedral-coordinated polynuclear polymolybdate MoO_3. Furthermore, carbon modification increased the alkalinity, reduced the acidity, and decreased the hydrophilicity of the catalyst surface. The carbon-modified catalysts contained more highly active sulfide phases, such as Mo-Ni-S and MoS_2, and the sulfidation degree increased with higher carbon content. Additionally, the average number of stacked layers and the average length of the active phase in the hydrogenation catalysts increased with carbon modification, leading to improved metal dispersion and greater exposure of active centers. Catalysts with higher levels of carbon modification demonstrated enhanced hydrogenation activity in both HDS and HDN. This work not only presents an effective carbon-modification strategy but also offers new insights for the design of industrial hydrogenation catalysts.

CRediT Authorship Contribution Statement

Zhenhui Lv: Methodology, Investigation, Data curation, Conceptualization. Jianan Li: Writing — review & editing, Writing — original draft, Formal analysis, Data curation. Tao Yang: Writing — review & editing, Project administration, Methodology. Yibao Li: Writing — review & editing, Resources, Funding acquisition, Formal analysis. Chong Peng: Writing — review & editing, Supervision, Resources, Project administration, Funding acquisition, Conceptualization.

Declaration of Competing Interest

The authors declare that they have no known competing financial interests or personal relationships that could have appeared to influence the work reported in this paper.

Acknowledgements

This work was supported by grants from the National Natural Science Foundation of China (22122807 and 22378038), Fundamental Research Funds for the Central Universities (DUT23RC(3)044), State Key Laboratory of Heavy Oil Processing, China University of Petroleum (WX20230149), the Double Thousand Plan of Jiangxi Province (jxsq2023102007) and China Postdoctoral Science Foundation (2024M750328).

Supplementary Material

Supplementary data to this article can be found online at https://doi.org/10.1016/j.cjche.2024.12.025.

Nomenclature

L	average slab length of MoS_2, nm
L_i	slab length of the ith MoS_2 unit, nm
N	stacking layer number of MoS_2
N_i	stacking layer number of the ith MoS_2
S_i	number of slabs or stacks in a determined range of the ith MoS_2
w_{N0}	the mass fractions of nitrogen in the raw material, $\mu g \cdot g^{-1}$
w_{N1}	the mass fractions of nitrogen in the product, $\mu g \cdot g^{-1}$
w_{S0}	the mass fractions of sulfur in the raw material, $\mu g \cdot g^{-1}$
w_{S1}	the mass fractions of sulfur in the product, $\mu g \cdot g^{-1}$

References

[1] M. Schwarzman, S. Schildroth, M. Bhetraratana, Á. Alvarado, J. Balmes, Raising standards to lower diesel emissions, *Science* 371 (6536) (2021) 1314–1316.
[2] G.F. Yang, Y. Zhang, X.N. Li, Impact of gasoline upgrade policy on particulate matter pollution in China, *J. Clean. Prod.* 262 (2020) 121336.
[3] F. Edition, Worldwide fuel charter [EB/OL]. http://www.acea.be/files/world_wide_fuel_charter_2006, 2013.

[4] W.X. Yu, L. Ye, X.L. Qin, A. Murad, J.C. Liu, Q. Ying, B. Xing, J.Q. Xie, L.X. Hou, Reaction behaviors of polycyclic aromatic hydrocarbon molecules in a diesel hydro-upgrading process based on the molecular-level reaction kinetic model, *Ind. Eng. Chem. Res.* 61 (17) (2022) 5723–5733.
[5] M.Y. Jin, M.E. Lee, M. Seo, J.K. Kim, S. Li, M. Choi, Coproduction of value-added lube base oil and green diesel from natural triglycerides *via* a simple two-step process, *Ind. Eng. Chem. Res.* 59 (19) (2020) 8946–8954.
[6] F. Chen, G.H. Zhang, X.Y. Weng, Y.H. Zhang, L. Zhao, L.Y. Cao, J.S. Gao, C.M. Xu, X.Q. Liu, X.H. Gao, High value utilization of inferior diesel for BTX production: mechanisms, catalysts, conditions and challenges, *Appl. Catal. Gen.* 616 (2021) 118095.
[7] R. Saab, K. Polychronopoulou, L.X. Zheng, S. Kumar, A. Schiffer, Synthesis and performance evaluation of hydrocracking catalysts: a review, *J. Ind. Eng. Chem.* 89 (2020) 83–103.
[8] Y.L. Jia, B.Y. Bai, J. Wang, Y.Y. Wang, Z. Wang, X.X. Ma, NiMo-MMO catalyst derived from LDHs precursors toward the deep hydrogenation of pyrene, *Chin. J. Chem. Eng.* 76 (2024) 201–210.
[9] S.D. Jaydev, A.J. Martín, J. Pérez-Ramírez, Direct conversion of polypropylene into liquid hydrocarbons on carbon-supported platinum catalysts, *ChemSusChem* 14 (23) (2021) 5179–5185.
[10] A. Allwar, N. Indriyani, R. Maulina, F. Rahmawati, Hydrocracking optimization of palm oil over $NiMoO_4$/activated carbon catalyst to produce biogasoline and kerosine, *Open Chem.* 20 (1) (2022) 1643–1652.
[11] K. Kohli, R. Prajapati, S.K. Maity, B.K. Sharma, Effect of silica, activated carbon, and alumina supports on NiMo catalysts for residue upgrading, *Energies* 13 (18) (2020) 4967.
[12] B.L. Tian, K.M. Dong, F.Q. Guo, S.B. Mao, J.M. Bai, R. Shu, L. Qian, Q. Liu, Catalytic conversion of toluene as a biomass tar model compound using monolithic biochar-based catalysts decorated with carbon nanotubes and graphic carbon covered Co-Ni alloy nanoparticles, *Fuel* 324 (2022) 124585.
[13] M.J. Angeles, C. Leyva, J. Ancheyta, S. Ramírez, A review of experimental procedures for heavy oil hydrocracking with dispersed catalyst, *Catal. Today* 220 (2014) 274–294.
[14] M.A. Ali, T. Tatsumi, T. Masuda, Development of heavy oil hydrocracking catalysts using amorphous silica-alumina and zeolites as catalyst supports, *Appl. Catal. Gen.* 233 (1–2) (2002) 77–90.
[15] R. de Haan, G. Joorst, E. Mokoena, C.P. Nicolaides, Non-sulfided nickel supported on silicated alumina as catalyst for the hydrocracking of *n*-hexadecane and of iron-based Fischer-Tropsch wax, *Appl. Catal. Gen.* 327 (2) (2007) 247–254.
[16] W.W. Feng, Y.G. Qian, T.H. Wang, Q.Y. Cui, Y.Y. Yue, P. Yuan, X.J. Bao, Impacts of support properties on the vacuum residue slurry-phase hydrocracking performance of Mo catalysts, *Pet. Sci.* 20 (4) (2023) 2575–2584.
[17] Y. Hao, D.J. Zhao, Y. Zhou, M.R. Yin, Z.Q. Wang, G.X. Xi, S.L. Song, Q.H. Tang, J. H. Yang, Hierarchical leaf-like alumina-carbon nanosheets with ammonia water modification for ethanol dehydration to ethylene, *Fuel* 333 (2023) 126128.
[18] Z. Liu, J.C. Yuan, Z.Z. Sun, X. Feng, Y.B. Liu, H.H. Zhu, C. Peng, C.H. Yang, Morphology effect on catalytic performance of ebullated-bed residue hydrotreating over Ni–Mo/Al_2O_3 catalyst: a kinetic modeling study, *Green Chem. Eng.* 5 (1) (2024) 60–67.
[19] Z.W. Liu, W. Han, D.W. Hu, H. Nie, Z. Wang, S.L. Sun, Z.H. Deng, Q.H. Yang, Promoting effects of SO_4^{2-} on a $NiMo/\gamma$-Al_2O_3 hydrodesulfurization catalyst, *Catal. Sci. Technol.* 10 (15) (2020) 5218–5230.
[20] C. Liu, J.L. Mei, G. Wang, J. Chang, Q. Meng, D. Hu, C.K. Xiao, Y. Shi, A.J. Duan, Y. J. Gong, Tailoring NiMoS active phases with high hydrodesulfurization activity through facilely synthesized supports with tunable mesostructure and morphology, *J. Catal.* 387 (2020) 170–185.
[21] Z.H. Lv, J.N. Li, D. Xue, T. Yang, G. Wang, C. Peng, Facile molybdenum and aluminum recovery from spent hydrogenation catalyst, *Chin. J. Chem. Eng.* 69 (2024) 72–78.
[22] L. Shi, Z.H. Zhang, Z.G. Qiu, F. Guo, W. Zhang, L.F. Zhao, Effect of phosphorus modification on the catalytic properties of Mo-Ni/Al_2O_3 in the hydrodenitrogenation of coal tar, *J. Fuel Chem. Technol.* 43 (1) (2015) 74–80.
[23] S.K. Maity, L. Flores, J. Ancheyta, H. Fukuyama, Carbon-modified alumina and alumina–carbon-supported hydrotreating catalysts, *Ind. Eng. Chem. Res.* 48 (3) (2009) 1190–1195.
[24] T. Lampke, B. Wielage, D. Dietrich, A. Leopold, Details of crystalline growth in co-deposited electroplated nickel films with hard (nano)particles, *Appl. Surf. Sci.* 253 (5) (2006) 2399–2408.
[25] D. Larissa Brito, D. François Payan, D. Florian Albrieux, D. Emmanuelle Guillon, P.J.A. Martens, D.G.D. Pirngruber, Hydrocracking of a long chain alkylcycloalkane: role of porosity and metal-acid balance, *ChemCatChem* 15 (5) (2023) e202201286.
[26] Z.K. Cao, X. Zhang, J.L. Mei, R. Guo, Z.M. Wu, S.D. Hou, S.Z. Peng, S.Q. Fan, C. Peng, A.J. Duan, Hydrocracking straight-Run diesel into high-value chemical materials: the effect of acidity and kinetic study, *Ind. Eng. Chem. Res.* 61 (25) (2022) 8685–8697.
[27] S.G.A. Ferraz, F.M.Z. Zotin, L.R.R. Araujo, J.L. Zotin, Influence of support acidity of NiMoS catalysts in the activity for hydrogenation and hydrocracking of tetralin, *Appl. Catal. Gen.* 384 (1–2) (2010) 51–57.
[28] T.B. Liu, P.L. Sun, H.H. Zhu, T. Yang, B.T. Tang, C. Peng, The effect of hydroxyl and metal synergetic structures on the FCC diesel hydrotreating performance of $NiMo/Al_2O_3$ catalysts, *Fuel* 356 (2024) 129487.
[29] J.K. Yang, T.J. Zuo, J.Y. Lu, Effect of preparation methods on the hydrocracking performance of $NiMo/Al_2O_3$ catalysts, *Chin. J. Chem. Eng.* 32 (2021) 224–230.
[30] D. Dhaneswara, J.F. Fatriansyah, T. Sudiro, S. Harjanto, M.S. Mastuli, A. Federico, R. Ulfiati, Synthesis and optimization of Ni/Mo-impregnated Kaolin-based ZSM-5 as a catalytic hydrocracking catalyst for heavy petroleum distillates, *Sustain. Energy Fuels* 8 (12) (2024) 2695–2703.
[31] X.N. Zhang, X.L. Huang, H. Huang, X.F. Wang, X.Y. Wang, Effect of Ni/Mo on the preparation of non-loaded $NiMoS_x$ catalysts and the hydrogenation performance of coal tar, *Fuel* 361 (2024) 130700.
[32] A.A. Salomatina, K.A. Nadeina, O.V. Klimov, I.G. Danilova, E.Y. Gerasimov, I.P. Prosvirin, V.P. Pakharukova, Y.A. Chesalov, A.S. Noskov, Influence of Ni/Mo ratio on structure formation of Ni-Mo complex compounds in $NiMo/Al_2O_3$ catalysts for selective diene hydrogenation, *Energy Fuels* 36 (2022) 15088–15099.